Ultrafast Dissociation of Water Producing Atomic Oxygen following Excitation above the O 1s Threshold

Florian Trinter,[1,*] Stephan Thürmer,[2] Qi Zhou (周琪),[1] Uwe Hergenhahn,[1] Bernd Winter,[1] Olle Björneholm,[3] Maxim Tchaplyguine,[4] Ludger Inhester,[5] and Gunnar Öhrwall[4,†]

[1]*Fritz-Haber-Institut der Max-Planck-Gesellschaft, Faradayweg 4-6, 14195 Berlin, Germany*
[2]*Department of Chemistry, Graduate School of Science, Kyoto University, Kitashirakawa-Oiwakecho, Sakyo-Ku, 606-8502 Kyoto, Japan*
[3]*Department of Physics and Astronomy, Uppsala University, Box 516, 75120 Uppsala, Sweden*
[4]*MAX IV Laboratory, Lund University, Box 118, 22100 Lund, Sweden*
[5]*Center for Free-Electron Laser Science CFEL, Deutsches Elektronen-Synchrotron DESY, Notkestraße 85, 22607 Hamburg, Germany*

(Received 10 December 2025; revised 16 July 2026; accepted 8 September 2026; published 5 November 2026)

We report ultrafast dissociation of gas-phase water following photoexcitation above the O 1s ionization threshold. High-resolution resonant Auger spectroscopy reveals sharp constant-kinetic-energy features arising from nonradiative decay of neutral atomic oxygen formed within the O 1s core-hole lifetime. Comparison with *ab initio* Auger spectra identifies these features as transitions from the atomic $(1s)^1(2s)^2(2p)^5\ ^1P$ state, demonstrating that neutral fragments can form in well-defined electronic states before Auger decay.

DOI: 10.1103/c1hm-82p2

Ultrafast dissociation (UFD) following core-level excitation, i.e., fragmentation occurring on timescales comparable to or shorter than the lifetime of the vacancy in the core level, typically a few fs or shorter, was first identified by Morin and Nenner in 1986 in electron spectra of core-excited HBr [1]. Since then, UFD has been extensively studied in systems ranging from simple diatomics to small polyatomic molecules, typically involving core excitation into antibonding orbitals [2–8].

In water, UFD has been observed under various conditions. The earliest direct evidence for UFD in molecular water came from studies of resonant Auger decay following excitation of the O $1s^{-1}4a_1$ state. Hjelte *et al.* demonstrated that core-excited H_2O molecules dissociate on a few-femtosecond (≈4 fs) timescale into core-excited OH fragments and neutral H atoms, producing "hot bands," features stemming from vibrationally excited OH, in the Auger spectra [9].

More recently, UFD features of H_2O have also been observed using resonant inelastic x-ray scattering (RIXS). Ertan *et al.* combined experiment and theory to show that RIXS spectra of gaseous water upon $4a_1$ excitation exhibit atomiclike narrow peaks, revealing signatures of nuclear dynamics (i.e., UFD) [10].

In a related study, Yamazoe *et al.* explored high overtones in the OH stretch region while approaching the continuum of bond breakage in liquid water via RIXS, quantifying how dissociative contributions evolve with excitation energy [11]. Identifying the impact of UFD on the water RIXS spectrum was essential for resolving the long-standing debate about whether the characteristic split of the $1b_1$ emission peak arises from two distinct structural motifs in liquid water [12].

Apart from water, UFD has been documented in molecules such as ammonia, halogenated ethanes, and other small polyatomics. In the case of the isoelectronic molecule NH_3, resonant Auger spectroscopy (following N $1s \rightarrow 4a_1$ excitation) revealed fragment bands whose spectral lines remain at constant electron kinetic energy (KE) when scanning the excitation across the resonance, characteristic of dissociation occurring before or during the decay process [7,13].

Similarly, Travnikova *et al.* studied "routes" to UFD in polyatomic systems, including the Auger-Doppler effects in fragmentation, confirming that core-excited states often dissociate on ultrafast timescales when populated into antibonding orbitals [5,7,14].

The above-mentioned cases of UFD all concerned excitation of a single electron into an antibonding orbital, but UFD after excitation into doubly excited states above the core-ionization threshold has been suggested to occur as well. One such case was N_2 [15], but a later high-resolution

*Contact author: trinter@fhi-berlin.mpg.de
†Contact author: gunnar.ohrwall@maxiv.lu.se

Published by the American Physical Society under the terms of the Creative Commons Attribution 4.0 International license. Further distribution of this work must maintain attribution to the author(s) and the published article's title, journal citation, and DOI. Open access publication funded by the Max Planck Society.

study showed that the observations were likely due to unresolved vibrational features from the N_2 molecule [16]. Building on earlier studies of H_2O dissociation, research into valence and core-level double excitations has also suggested rapid fragmentation channels. Experiments involving electron impact and synchrotron radiation excitation have provided evidence for H atom fragments with high KE, which were interpreted as originating from doubly excited states that quickly dissociate into three neutral fragments [O in a $(2p)^4$ configuration, one excited H atom, and one H in the ground state] [17,18].

In water, UFD following core excitation into the antibonding $4a_1$ orbital is well established. However, it has also been proposed that excitation to doubly excited states, with one hole in the core orbital and one in a valence orbital, *above* the O 1s ionization threshold might lead to dissociation behavior. Piancastelli *et al.* made this proposal based on observations of constant-KE features and apparent vibrational structure, which they assigned to OH fragments produced by UFD from such doubly excited states [19].

In contrast, our results demonstrate that UFD from doubly excited molecular states above the O 1s threshold produces *neutral atomic oxygen* fragments rather than OH fragments. The process is depicted in Fig. 1 based on calculated potential-energy curves. Via photoexcitation and shakeup, the $(1a_1)^{-1}(3a_1)^{-1}(4a_1)^2$ state is populated, leading to the immediate dissociation of two H atoms. To our knowledge, single-photon excitation leading to the immediate dissociation of two atomic fragments within the core-hole lifetime has not been previously reported. This double dissociation has several important implications for core-excited molecular dynamics, notably advancing the understanding of possible dissociation pathways and motivating refined theoretical descriptions of the potential-energy surfaces of core-excited and doubly excited states.

Photoemission spectra of gaseous water, containing the Auger and resonant Auger region on a dense grid of photon energies, were recorded at the P04 soft x-ray beamline [20] of the PETRA III synchrotron-radiation facility (Deutsches Elektronen-Synchrotron, DESY, Hamburg, Germany) using the EASI setup [21]. Additional, polarization-dependent electron spectra were recorded at the photoemission end station of the low-density matter branch of the FlexPES beamline [22] (MAX IV, Lund, Sweden). Detailed experimental procedures are provided in Supplemental Material [23] (see also Refs. [24–29] therein).

Autoionization spectra were calculated for the water molecule and the atomic oxygen fragment employing the one-center approximation [30,31]. Calculations for the ^{3}P state and additional methodological details are provided in Supplemental Material [23] (see also Refs. [32–39] therein).

In Fig. 2(a), we present a false-color map of electron spectra covering KEs between 509 and 521 eV and photon energies between 547 and 552.5 eV, well above water's

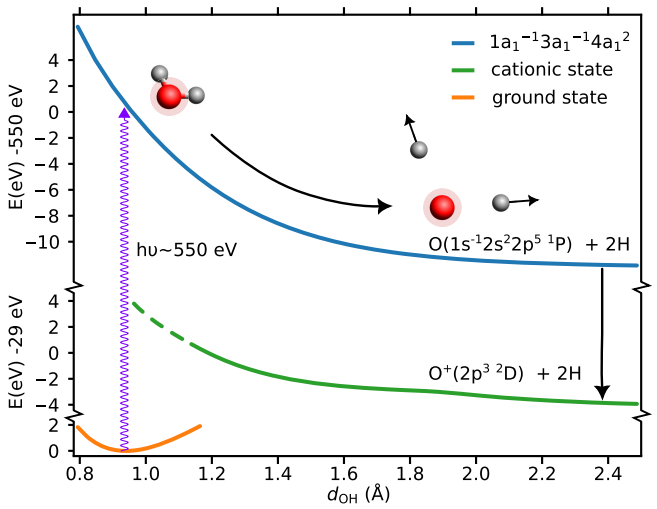


FIG. 1. Calculated potential-energy curves along the symmetric stretch coordinate. The energy is given relative to the equilibrium geometry of the neutral ground state. The blue curve shows the doubly excited $(1a_1)^{-1}(3a_1)^{-1}(4a_1)^2$ state, which is populated via core-electron excitation accompanied by shakeup from the ground state (orange curve) at a photon energy of 550 eV. This strongly repulsive state leads to ultrafast dissociation into atomic fragments: an oxygen atom in the $(1s)^1(2s)^2(2p)^5$ ^{1}P state and two hydrogen atoms in their ground states. The state subsequently undergoes electronic decay into several cationic states; for example, the green curve depicts a state that asymptotically corresponds to an oxygen atom in the $(1s)^2(2s)^2(2p)^3$ ^{2}D state.

vertical O 1s ionization potential of 539.83 eV [40]. A constant-intensity photoelectron feature that disperses with photon energy is observed in this photon-energy range, which arises primarily from ionization of the $2a_1$ inner-valence orbital of H_2O but also includes contributions from two-hole-one-particle (2h-1p) states, overlapping in energy. This feature has been subtracted in an analogous but higher-resolution map shown in Fig. 2(d), from which the integrated electron energy [Fig. 2(b)] and absorption [Fig. 2(c)] spectra were produced. In Fig. 2(a), two weak and sharp features at constant KE can be seen at 511.4(1) and 513.1(1) eV. Their full width at half maximum (FWHM) is very similar, 0.35(2) and 0.34(2) eV, corresponding to ≈0.29 and ≈0.275 eV after deconvolution of the spectrometer contribution. They are most intense at a photon energy of $h\nu = 550.2(2)$ eV [compare Fig. 2(c)], and are populated over a photon-energy range of 4.55(1) eV (FWHM). All features have been fitted using exponentially modified Gaussian (EMG) peak shapes.

The constant KE of these resonant peaks indicates that they arise from electronic decay processes decoupled from the primary photoionization. In the study by Piancastelli *et al.* [19], these features were attributed to decays of neutral, core-excited OH fragments, produced by ultrafast dissociation of water molecules following photoexcitation to a doubly excited state. This conclusion was based on

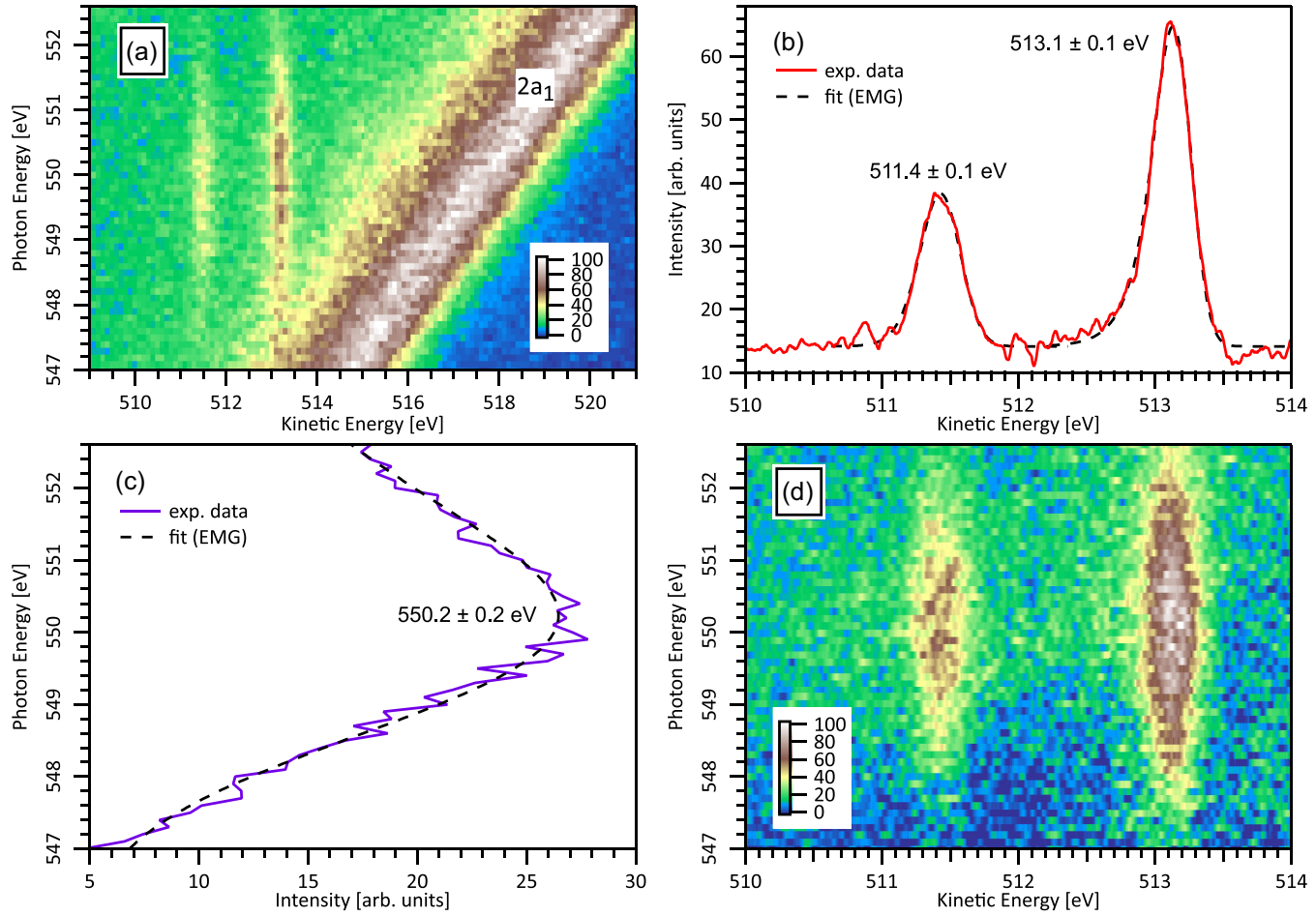


FIG. 2. (a) Electron spectra mapped as a function of photon energy around the features of interest, shown on calibrated photon-energy (left) and KE (bottom) scales, recorded at beamline P04 approximately at the "magic angle" (130° tilted with respect to the photon-beam axis [21]). Two resonant features with constant KE are observed, while the dispersive feature originates from photoionization of the $2a_1$ orbital. (b) Photoemission spectrum of the resonant features obtained by integrating over the full photon-energy range of the map in panel (d). (c) Photoabsorption spectrum derived by integrating over the shown KE range of the map in panel (d). (d) High-resolution scan of the resonant feature, with the signal contribution from the $2a_1$ orbital subtracted. The features in (b),(c) have been fitted using exponentially modified Gaussian (EMG) profiles.

both the constant KE of the peaks and the apparent vibrational structure observed in their spectra.

In the spectrum shown in Fig. 2(b), which exhibits less noise than those reported in Ref. [19], no discernible vibrational structure is observed in the peaks, although a slight asymmetry toward higher KEs is apparent. The vibrational spacing in OH^+ is expected to be on the order of 400 meV for the lowest electronic states [9], which is well within the resolution capability of the spectrometer. Additional data recorded at the FlexPES beamline of MAX IV also show no discernible vibrational structure (see Fig. 3 and Fig. S1 in Supplemental Material [23]).

The narrow linewidth and absence of vibrational structure instead suggest that the peaks originate from nonradiative decay within an atomic fragment. In this scenario, the slight asymmetry can be attributed to decays occurring at different points along the dissociation pathway on the potential-energy surface of the core-excited state, which, in general, is not parallel to the one of the respective final state.

The emergence of the atomic decay spectrum from the molecular Auger spectrum along the ultrafast dissociation pathway following shakeup into the $(1a_1)^1(1b_2)^2(3a_1)^1(1b_1)^2(4a_1)^2\ {}^1A_1$ configuration is explained in the End Matter and in Supplemental Material Sec. V [23]. We confirm that signatures of molecular Auger decay are barely visible owing to the substantial line broadening and strong energy shifts that occur during dissociation. Ultimately, the only observable features are the sharp atomic lines originating from the oxygen atom.

The energies of core-hole resonant Auger decays from photoexcited O atoms were determined experimentally by Caldwell *et al.* [41]. Following the optically allowed excitation from the $(1s)^2(2s)^2(2p)^4\ {}^3P$ ground state to the $(1s)^1(2s)^2(2p)^5\ {}^3P$ core-excited state, the spacing between the two lowest observed final states reached by

Auger decay, $(1s)^2(2s)^2(2p)^3\ ^2D$ and $(1s)^2(2s)^2(2p)^3\ ^2P$, was found to be 1.68 eV. This exactly matches the separation of the peaks we observe, while the absolute energies found in Ref. [41], 510.12 and 508.44 eV, respectively, are lower by about 3 eV. As a cross-check, the expected KE for these transitions can be estimated to be 510.32 and 508.62 eV from the difference between the excitation energy of the $(1s)^1(2s)^2(2p)^5\ ^3P$ state (527.26 eV [42]) and the ionization thresholds of the final states [16.94 and 18.64 eV for the $(1s)^2(2s)^2(2p)^3\ ^2D$ and ^2P states, respectively [43]], in reasonable agreement with the values in Ref. [41].

As anticipated from the calculated potential-energy curve in Fig. 1, the electrons originate from the decay of a higher-lying core-excited state of the oxygen atom, namely, the $(1s)^1(2s)^2(2p)^5\ ^1P$ state. This state has been theoretically estimated to lie between 2.71 and 3.01 eV above the ^3P state [2,44,45], bringing the calculated energy separation close to our observation. Thus, a consistent interpretation is that the observed features arise from electronic decays of a neutral oxygen fragment in the $(1s)^1(2s)^2(2p)^5\ ^1P$ core-excited state into the $(1s)^2(2s)^2(2p)^3\ ^2D$ and ^2P final states.

We can further support this interpretation by examining additional final-state features expected to appear in the decay spectrum. A complication is that the energy range where these final states would appear is dominated by molecular water KVV (core-valence-valence) Auger features. To overcome this issue, we recorded spectra at the FlexPES beamline over a broader range of KEs at photon energies of 545 eV (below the onset of these resonant features) and 550 eV (near the maximum) and constructed a difference spectrum. In Fig. 3, we show the outcome for two angles with respect to the horizontal linear light polarization, 90° (vertical) and 54.7° ("magic angle"). For a clearer comparison of the difference spectra between these two angles, we have subtracted the contribution from $2a_1$ photoemission from the spectra recorded at 54.7°; this contribution is already strongly suppressed in the 90° spectrum due to its large positive β value. The peaks attributed to decays of atomic oxygen generally exhibit relatively isotropic angular distributions, with the exception of the $(1s)^2(2s)^2(2p)^3\ ^2D$ state, which has $\beta = -0.51(5)$. This negative value can be attributed to orientation selection resulting from the molecular dissociation (see Supplemental Material [23] and Ref. [46] therein).

In addition, we plot orange bars in Fig. 3 corresponding to calculated positions and relative intensities for the most intense decays of atomic oxygen excited to the $(1s)^1(2s)^2(2p)^5\ ^1P$ state and labeled by their assignments of the final states. In the difference spectra, two sharp peaks appear at approximately 477.4 eV and 490.1 eV KE, in addition to those at 511.4 and 513.1 eV. The calculated estimates for the most intense decays are close to these peaks, and the relative intensities are well reproduced

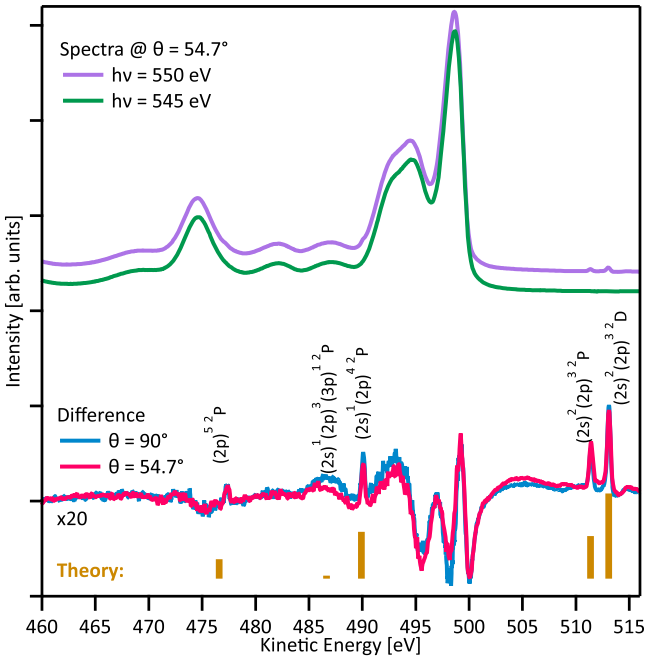


FIG. 3. Top: electron spectra recorded at 54.7° relative to the light polarization using photon energies of $h\nu = 545$ eV (green curve) and $h\nu = 550$ eV (purple curve); the $2a_1$ feature has been subtracted from the spectra (see Supplemental Material for details [23]). Bottom: the blue and red curves show the difference spectra (550 eV − 545 eV) for 90° (Auger spectra not shown above) and 54.7°, respectively, multiplied by a factor of 20. Four peaks, which we attribute to atomic oxygen, can be observed. The orange bars indicate the calculated positions and relative intensities of the strongest decays of atomic oxygen excited to the $(1s)^1(2s)^2(2p)^5\ ^1P$ state, labeled according to their final states.

(see Table I). The energy spacings between the peaks at 477.4 and 490.1 eV are also nearly identical to those reported by Caldwell *et al.* for features assigned to the $(1s)^2(2p)^5\ ^2P$ and $(1s)^2(2s)^1(2p)^4\ ^2P$ final states, respectively. These differences are reflected in our simulations of decays from the latter state, which are presented in Supplemental Material [23].

The emergence of these sharp peaks at a photon energy of 550 eV confirms their resonant character. The agreement between the observed peaks and the calculated spectrum for the ^1P excited state of atomic oxygen and the near-perfect agreement in the energy spacing to that reported by Caldwell *et al.* confirms their assignment to core-excited neutral oxygen fragments. The core-excited state cannot be accessed directly via dipole excitation from the O $(1s)^2(2s)^2(2p)^4\ ^3P$ ground state, but can clearly be populated through dissociation of the core-excited water molecule.

The singlet-triplet splitting estimated from our self-consistent-field calculations is 2.61 eV, slightly smaller than earlier estimates based on configuration-interaction calculations [44,45] and on the analogy with (isoelectronic) atomic neon [2]. We note that this value implies an excitation energy of the $(1s)^1(2s)^2(2p)^5\ ^3P$ state of

TABLE I. Kinetic energies (KE), relative energies (ΔE), and relative intensities (Int) obtained from the difference spectrum recorded at 54.7° with respect to the polarization, shown in Fig. 3, compared with results from our calculations for the $(1s)^1(2s)^2(2p)^5$ ^1P state Auger spectrum, including the angular parameter value l (superscript a), and experimental values for decays from the $(1s)^1(2s)^2(2p)^5$ ^3P state (superscript b) [41]. All energies are given in eV.

Final state	KE	ΔE	Int	KE^a	ΔE^a	Int^a	l^a	ΔE^b	Int^b
$(2s)^2(2p)^3$ ^2D	513.1(1)	0	1	513.09	0	1	2	0	1
$(2s)^2(2p)^3$ ^2P	511.42	1.68(1)	0.55(2)	511.39	1.70	0.49	0, 2	1.68	0.551
$(2s)^1(2p)^4$ ^2P	490.08	23.02(4)	0.43(10)	489.92	23.17	0.55	1	22.99	0.219
$(2s)^2(2p)^2(3p)^1$ ^2P	…	…	…	486.66	26.43	0.05	1	…	…
$(2s)^0(2p)^5$ ^2P	477.36	35.74(9)	0.19(10)	476.61	36.48	0.23	0, 2	35.80	0.24

≈527.4 eV, which is in good agreement with the most recent high-precision laboratory measurement of 527.26(4) eV by Leutenegger *et al.* [42].

In summary, we have demonstrated that photoexcitation of gaseous water significantly above the oxygen 1s ionization threshold can lead to the ultrafast formation of neutral atomic oxygen fragments. High-resolution resonant Auger electron spectroscopy reveals two sharp, constant-KE features whose energies, widths, and absence of vibrational structure are inconsistent with previously proposed core-hole decays of OH fragments. Instead, our experimental data, supported by molecular and atomic Auger energy calculations, unambiguously identify these features as electronic decays of atomic oxygen in the $(1s)^1(2s)^2(2p)^5$ ^1P state to the $(1s)^2(2s)^2(2p)^3$ ^2D and ^2P final states. Additional measurements uncovered the $(1s)^2(2p)^5$ ^2P and $(1s)^2(2s)^1(2p)^4$ ^2P final states, hidden below the much more intense molecular water KVV Auger features.

The photon-energy region in which we observe UFD has previously been investigated by photon-energy-dependent ion-yield spectroscopy with sensitivity to both cations and anions [47,48]. At the same photon energy of 550 eV we discuss here, an increase in the yield of negatively charged oxygen ions, O^-, is apparent. By calculations, Stråhlman *et al.* assign these to the decay of doubly excited states with a $(1s)^{-1}v^{-1}4a_1{}^2$ configuration, where v designates an outer-valence orbital. Due to the strongly antibonding character of the $4a_1$ orbital, these same states could be responsible for the UFD we observe here. In the anion yield, one would then observe the fraction of the states which has not undergone UFD, as some charge exchange between the oxygen and the protons seems to be necessary for creation of the O^- fragment.

This finding establishes a new form of ultrafast double dissociation, in which both O–H bonds rupture within the lifetime of the O 1s cole hole, producing neutral O fragments prior to Auger decay in the unique near-threshold photon-energy regime of 550.2 ± 4.55 eV explored here, where nuclear motion can outpace electronic relaxation processes. These results challenge earlier interpretations of high-energy UFD features in water and highlight the need to refine theoretical descriptions of core-excited and doubly excited potential-energy surfaces.

Our identification of atomic-fragment Auger emission following molecular core excitation reveals a previously unrecognized fragmentation channel in water that may also occur in other small molecules. This mechanism provides a benchmark for the interplay between electronic decay and nuclear motion on few-femtosecond timescales and has implications for radiation-induced chemistry in aqueous and atmospheric environments. Although our study focuses on isolated gas-phase water, similar ultrafast decay pathways could occur in small clusters or in the upper atmosphere. Even the extremely short-lived (≈4 fs) formation of neutral atomic oxygen may influence the earliest stages of chemical reactivity, highlighting a prototypical channel through which electronic decay couples to molecular fragmentation.

Extending such studies into the time domain remains challenging. Resolving Auger electron dynamics requires subfemtosecond pulses and, therefore, essentially attosecond x-ray pump-probe schemes, which are only now becoming feasible. To date, time-resolved Auger studies remain scarce (Refs. [49,50]), while current x-ray pump-probe experiments mainly probe nuclear dynamics on the tens-of-femtoseconds timescale. Direct access to electronic decay will enable real-time tracking of correlated electron motion and provide stringent tests of theory.

Neutral atomic oxygen acts as a highly reactive electrophilic species that readily attacks other compounds. Atomic oxygen is usually not considered to play a significant role in biological radiation damage, as any atoms produced would react rapidly with the surrounding water. In less dense and more radiation-intense environments, such as the Earth's mesosphere and lower thermosphere, however, atomic oxygen is important for photochemistry and energy balance (see, for example, Ref. [51]). This includes the formation of other reactive oxygen species (ROS), i.e., highly reactive oxygen-containing molecules and free radicals. For example, atomic oxygen can react with molecular oxygen to form

ozone via $O + O_2 \rightarrow O_3$. Reactions with water may produce hydroxyl radicals via $O + H_2O \rightarrow 2\,^{\cdot}OH$ or hydrogen peroxide via $O + H_2O \rightarrow H_2O_2$. All three $ROS - {}^{\cdot}OH$, O_3, and H_2O_2—are highly reactive, making the formation of atomic oxygen a potential starting point for cascading chemical reactions.

Acknowledgments—We acknowledge DESY (Hamburg, Germany), a member of the Helmholtz Association HGF, for the provision of experimental facilities. Parts of this research were carried out at PETRA III. We would like to thank Moritz Hoesch and his team for assistance during the experiments. Beamtime was allocated for proposal H-20010092. We acknowledge Jens Buck, Florian Diekmann, Matthias Kalläne, and Sebastian Rohlf from Christian-Albrechts-Universität zu Kiel for providing us with software to scan the photon energy via our SCIENTA spectrometer software. The authors acknowledge the MAX IV Laboratory for beamtime on the FlexPES beamline under proposal 20240548. Research conducted at MAX IV, a Swedish national user facility, is supported by Vetenskapsrådet (Swedish Research Council, VR) under Contract No. 2018-07152, Vinnova (Swedish Governmental Agency for Innovation Systems) under Contract No. 2018-04969, and Formas under Contract No. 2019-02496. F. T. and Q. Z. acknowledge funding by the Deutsche Forschungsgemeinschaft (DFG, German Research Foundation)—Project No. 509741550, Emmy Noether Programme. S. T. acknowledges support from the JSPS KAKENHI Grant No. JP25K08560. U. H. and B. W. acknowledge funding from the European Research Council (ERC) under the European Union's Horizon 2020 research and innovation program under Grant Agreement No. GAP 883759—AQUACHIRAL. O. B. acknowledges funding from the Swedish Research Council (VR) through the Project No. VR 2023-04346. L. I. acknowledges the scientific exchange and support of the Centre for Molecular Water Science (CMWS). L. I. further acknowledges support from DESY, a member of the Helmholtz Association HGF, and the Cluster of Excellence "CUI: Advanced Imaging of Matter" of the Deutsche Forschungsgemeinschaft (DFG)–EXC 2056–project ID 390715994.

Data availability—The data that support the findings of this study are openly available in the Zenodo data repository at [52].

[1] P. Morin and I. Nenner, Atomic autoionization following very fast dissociation of core-excited HBr, Phys. Rev. Lett. **56**, 1913 (1986).

[2] S. J. Schaphorst, C. D. Caldwell, M. O. Krause, and J. Jiménez-Mier, Evidence for atomic features in the decay of resonantly excited molecular oxygen, Chem. Phys. Lett. **213**, 315 (1993).

[3] A. Menzel, B. Langer, J. Viefhaus, S. B. Whitfield, and U. Becker, Competition between direct dissociation and resonant Auger decay: A quasi-classical model applied to the $2p^{-1}\sigma^*$ states of HCl, DCl and Cl_2, Chem. Phys. Lett. **258**, 265 (1996).

[4] O. Björneholm, M. Bässler, A. Ausmees, I. Hjelte, R. Feifel, H. Wang, C. Miron, M. N. Piancastelli, S. Svensson, S. L. Sorensen, F. Gel'mukhanov, and H. Ågren, Doppler splitting of in-flight Auger decay of dissociating oxygen molecules: The localization of delocalized core holes, Phys. Rev. Lett. **84**, 2826 (2000).

[5] O. Travnikova, V. Kimberg, R. Flammini, X.-J. Liu, M. Patanen, C. Nicolas, S. Svensson, and C. Miron, On routes to ultrafast dissociation of polyatomic molecules, J. Phys. Chem. Lett. **4**, 2361 (2013).

[6] H. Sann *et al.*, Imaging the temporal evolution of molecular orbitals during ultrafast dissociation, Phys. Rev. Lett. **117**, 243002 (2016).

[7] O. Travnikova, E. Kukk, F. Hosseini, S. Granroth, E. Itälä, T. Marchenko, R. Guillemin, I. Ismail, R. Moussaoui, L. Journel, J. Bozek, R. Püttner, P. Krasnov, V. Kimberg, F. Gel'mukhanov, M. N. Piancastelli, and M. Simon, Ultrafast dissociation of ammonia: Auger Doppler effect and redistribution of the internal energy, Phys. Chem. Chem. Phys. **24**, 5842 (2022).

[8] M. Hrast, M. Ljubotina, and M. Žitnik, *Ab initio* Auger spectrum of the ultrafast dissociating $2p_{3/2}{}^{-1}\sigma^*$ resonance in HCl, Phys. Chem. Chem. Phys. **27**, 1473 (2025).

[9] I. Hjelte, M. N. Piancastelli, R. F. Fink, O. Björneholm, M. Bässler, R. Feifel, A. Giertz, H. Wang, K. Wiesner, A. Ausmees, C. Miron, S. L. Sorensen, and S. Svensson, Evidence for ultra-fast dissociation of molecular water from resonant Auger spectroscopy, Chem. Phys. Lett. **334**, 151 (2001).

[10] E. Ertan, V. Savchenko, N. Ignatova, V. Vaz da Cruz, R. C. Couto, S. Eckert, M. Fondell, M. Dantz, B. Kennedy, T. Schmitt, A. Pietzsch, A. Föhlisch, F. Gel'mukhanov, M. Odelius, and V. Kimberg, Ultrafast dissociation features in RIXS spectra of the water molecule, Phys. Chem. Chem. Phys. **20**, 14384 (2018).

[11] K. Yamazoe, J. Miyawaki, H. Niwa, A. Nilsson, and Y. Harada, Measurements of ultrafast dissociation in resonant inelastic x-ray scattering of water, J. Chem. Phys. **150**, 204201 (2019).

[12] S. Li *et al.*, Attosecond-pump attosecond-probe x-ray spectroscopy of liquid water, Science **383**, 1118 (2024).

[13] I. Hjelte, M. N. Piancastelli, C. M. Jansson, K. Wiesner, O. Björneholm, M. Bässler, S. L. Sorensen, and S. Svensson, Evidence of ultra-fast dissociation in ammonia observed by resonant Auger electron spectroscopy, Chem. Phys. Lett. **370**, 781 (2003).

[14] O. Kugeler, G. Prümper, R. Hentges, J. Viefhaus, D. Rolles, U. Becker, S. Marburger, and U. Hergenhahn, Intramolecular electron scattering and electron transfer following autoionization in dissociating molecules, Phys. Rev. Lett. **93**, 033002 (2004).

[15] M. Neeb, A. Kivimäki, B. Kempgens, H. M. Köppe, J. Feldhaus, and A. M. Bradshaw, Core hole double-excitation and atomiclike Auger decay in N_2, Phys. Rev. Lett. **76**, 2250 (1996).

[16] A. Naves de Brito, I. Hjelte, K. Wiesner, R. Feifel, M. Bässler, S. L. Sorensen, O. Björneholm, M. N. Piancastelli, L. Karlsson, and S. Svensson, Evidence against atomiclike resonant Auger decay in N_2 doubly excited core states by high-resolution experiments, Phys. Rev. A **64**, 054702 (2001).

[17] N. Kouchi, K. Ito, Y. Hatano, N. Oda, and T. Tsuboi, Translational spectroscopy of electron-impact dissociative excitation of H_2O and D_2O by doppler profile measurements of Balmer-α emission, Chem. Phys. **36**, 239 (1979).

[18] Y. Hatano, Interaction of vacuum ultraviolet photons with molecules. Formation and dissociation dynamics of molecular superexcited states, Phys. Rep. **313**, 109 (1999).

[19] M. N. Piancastelli, R. Sankari, S. Sorensen, A. De Fanis, H. Yoshida, M. Kitajima, H. Tanaka, and K. Ueda, Resonant Auger decay of above-threshold core-excited H_2O, Phys. Rev. A **71**, 010703(R) (2005).

[20] J. Viefhaus, F. Scholz, S. Deinert, L. Glaser, M. Ilchen, J. Seltmann, P. Walter, and F. Siewert, The variable polarization XUV beamline P04 at PETRA III: Optics, mechanics and their performance, Nucl. Instrum. Methods Phys. Res., Sect. A **710**, 151 (2013).

[21] S. Malerz, H. Haak, F. Trinter, A. B. Stephansen, C. Kolbeck, M. Pohl, U. Hergenhahn, G. Meijer, and B. Winter, A setup for studies of photoelectron circular dichroism from chiral molecules in aqueous solution, Rev. Sci. Instrum. **93**, 015101 (2022).

[22] A. Preobrajenski, A. Generalov, G. Öhrwall, M. Tchaplyguine, H. Tarawneh, S. Appelfeller, E. Frampton, and N. Walsh, FlexPES: A versatile soft X-ray beamline at MAX IV Laboratory, J. Synchrotron Radiat. **30**, 831 (2023).

[23] See Supplemental Material at http://link.aps.org/supplemental/10.1103/c1hm-82p2 for experimental details, energy balance, angle-resolved electron spectra and anisotropy parameters, subtraction of the $2a_1$ signal, and Auger spectrum calculations.

[24] A. Hiraya, K. Nobusada, M. Simon, K. Okada, T. Tokushima, Y. Senba, H. Yoshida, K. Kamimori, H. Okumura, Y. Shimizu, A.-L. Thomas, P. Millie, I. Koyano, and K. Ueda, H_2^+ formation from H_2O^+ mediated by the core-excitation-induced nuclear motion in H_2O, Phys. Rev. A **63**, 042705 (2001).

[25] S. Y. Truong, A. J. Yencha, A. M. Juarez, S. J. Cavanagh, P. Bolognesi, and G. C. King, Threshold photoelectron spectroscopy of H_2O and D_2O over the photon energy range 12–40 eV, Chem. Phys. **355**, 183 (2009).

[26] J. Buck, K. Bagschik, L. Glaser, F. Scholz, J. Seltmann, and J. Viefhaus, Progress report on the XUV online diagnostic unit for the highly accurate determination of SR properties, AIP Conf. Proc. **2054**, 060057 (2019).

[27] E. Kukk, G. Snell, J. D. Bozek, W.-T. Cheng, and N. Berrah, Vibrational structure and partial rates of resonant Auger decay of the N 1s $\rightarrow 2\pi$ core excitations in nitric oxide, Phys. Rev. A **63**, 062702 (2001).

[28] E. Kukk, K. Ueda, U. Hergenhahn, X.-J. Liu, G. Prümper, H. Yoshida, Y. Tamenori, C. Makochekanwa, T. Tanaka, M. Kitajima, and H. Tanaka, Violation of the Franck-Condon principle due to recoil effects in high energy molecular core-level photoionization, Phys. Rev. Lett. **95**, 133001 (2005).

[29] J. L. Campbell and T. Papp, Widths of the atomic K-N7 levels, At. Data Nucl. Data Tables **77**, 1 (2001).

[30] H. Ågren, S. Svensson, and U. I. Wahlgren, SCF and limited CI calculations for assignment of the Auger spectrum and of the satellites in the soft X-ray spectrum of H_2O, Chem. Phys. Lett. **35**, 336 (1975).

[31] H. Siegbahn, L. Asplund, and P. Kelfve, The Auger electron spectrum of water vapour, Chem. Phys. Lett. **35**, 330 (1975).

[32] Y. Hao, L. Inhester, K. Hanasaki, S.-K. Son, and R. Santra, Efficient electronic structure calculation for molecular ionization dynamics at high x-ray intensity, Struct. Dyn. **2**, 041707 (2015).

[33] L. Inhester, K. Hanasaki, Y. Hao, S.-K. Son, and R. Santra, X-ray multiphoton ionization dynamics of a water molecule irradiated by an x-ray free-electron laser pulse, Phys. Rev. A **94**, 023422 (2016).

[34] S.-K. Son, L. Young, and R. Santra, Impact of hollow-atom formation on coherent x-ray scattering at high intensity, Phys. Rev. A **83**, 033402 (2011).

[35] Z. Jurek, S.-K. Son, B. Ziaja, and R. Santra, *XMDYN* and *XATOM*: Versatile simulation tools for quantitative modeling of X-ray free-electron laser induced dynamics of matter, J. Appl. Crystallogr. **49**, 1048 (2016).

[36] T. H. Dunning, Jr., Gaussian basis sets for use in correlated molecular calculations. I. The atoms boron through neon and hydrogen, J. Chem. Phys. **90**, 1007 (1989).

[37] L. Inhester, C. F. Burmeister, G. Groenhof, and H. Grubmüller, Auger spectrum of a water molecule after single and double core ionization, J. Chem. Phys. **136**, 144304 (2012).

[38] T. Marchenko, L. Inhester, G. Goldsztejn, O. Travnikova, L. Journel, R. Guillemin, I. Ismail, D. Koulentianos, D. Céolin, R. Püttner, M. N. Piancastelli, and M. Simon, Ultrafast nuclear dynamics in the doubly-core-ionized water molecule observed via Auger spectroscopy, Phys. Rev. A **98**, 063403 (2018).

[39] I. Ismail *et al.*, Ultrafast nuclear dynamics in double-core-ionized water molecules, Phys. Rev. A **110**, 013108 (2024).

[40] P. Wang, T. X. Carroll, T. D. Thomas, L. J. Sæthre, and K. J. Børve, Calibration of oxygen 1s ionization energies. Accurate energies for CO_2, H_2O, CO, and O_2, J. Electron Spectrosc. Relat. Phenom. **251**, 147103 (2021).

[41] C. D. Caldwell, S. J. Schaphorst, M. O. Krause, and J. Jiménez-Mier, Photoexcited *K* Auger spectra of atomic and molecular oxygen, J. Electron Spectrosc. Relat. Phenom. **67**, 243 (1994).

[42] M. A. Leutenegger *et al.*, High-precision determination of oxygen K_α transition energy excludes incongruent motion of interstellar oxygen, Phys. Rev. Lett. **125**, 243001 (2020).

[43] A. Kramida, Y. Ralchenko, J. Reader, and NIST ASD Team, NIST Atomic Spectra Database (ver. 5.12), [Online]. Available: https://physics.nist.gov/asd, National Institute of Standards and Technology, Gaithersburg, MD, USA (2024).

[44] A. Yagishita, E. Shigemasa, and N. Kosugi, Observation of Rydberg-valence mixing in high-resolution symmetry-resolved oxygen *K*-edge spectra of O_2, Phys. Rev. Lett. **72**, 3961 (1994).

[45] M. Eroms, O. Vendrell, M. Jungen, H.-D. Meyer, and L. S. Cederbaum, Nuclear dynamics during the resonant Auger decay of water molecules, J. Chem. Phys. **130**, 154307 (2009).

[46] N. M. Kabachnik, J. Tulkki, H. Aksela, and S. Ricz, Coherence and correlation in the anisotropy of Ne $KL-LLL$ satellite Auger decay, Phys. Rev. A **49**, 4653 (1994).
[47] W. C. Stolte, M. M. Sant'Anna, G. Öhrwall, I. Dominguez-Lopez, M. N. Piancastelli, and D. W. Lindle, Photofragmentation dynamics of core-excited water by anion-yield spectroscopy, Phys. Rev. A **68**, 022701 (2003).
[48] C. Stråhlman, B. Moog, E. Ertan, M. Odelius, A. Kivimäki, R. Richter, and R. Sankari, Selective negative-ion formation from core-valence doubly excited states of the water molecule, Phys. Rev. A **98**, 053432 (2018).
[49] D. C. Haynes *et al.*, Clocking Auger electrons, Nat. Phys. **17**, 512 (2021).
[50] M. Hasan, J. Gao, H. Liang, Y. Yuan, Z. Eisenhutt, M.-S. Tsai, M.-C. Chen, H. J. Wörner, A. Rudenko, and M. Han, Time-domain measurement of Auger electron dynamics in xenon and krypton atoms after giant resonance photoionization, Phys. Rev. Lett. **136**, 163201 (2026).
[51] H. Richter, C. Buchbender, R. Güsten, R. Higgins, B. Klein, J. Stutzki, H. Wiesemeyer, and H.-W. Hübers, Direct measurements of atomic oxygen in the mesosphere and lower thermosphere using terahertz heterodyne spectroscopy, Commun. Earth Environ. **2**, 19 (2021).
[52] 10.5281/zenodo.17866759.

End Matter

Figure 4 depicts calculated instantaneous Auger spectra $T(E,t)$ at selected times (see Supplemental Material Sec. V [23]), as well as the resulting Auger spectrum $T(E)$ (brown curve, termed "convoluted"). For comparison, we also show the atomic spectrum corresponding to the ^{1}P core-excited state. Note that the atomic peak at 490 eV differs slightly from the asymptotic molecular peak because a somewhat smaller configurational space was employed in the molecular calculations. The time-resolved Auger spectra clearly illustrate how the spectrum evolves from molecular to atomic character, accompanied by substantial shifts of the spectral lines. The high-energy contribution at 520 eV is associated with decay processes involving electrons in the $4a_1$ orbital. These transitions are suppressed as the hydrogen atoms dissociate from the molecule. The resulting spectrum is thus a mixture of contributions from the transient molecular species and the final atomic fragment. However, the molecular component is extremely broad because the wave packet, when projected onto the steep potential-energy curves (see Fig. 1), spans a wide range of energies for each decay transition. During dissociation, this broadening mechanism becomes less pronounced as the potential-

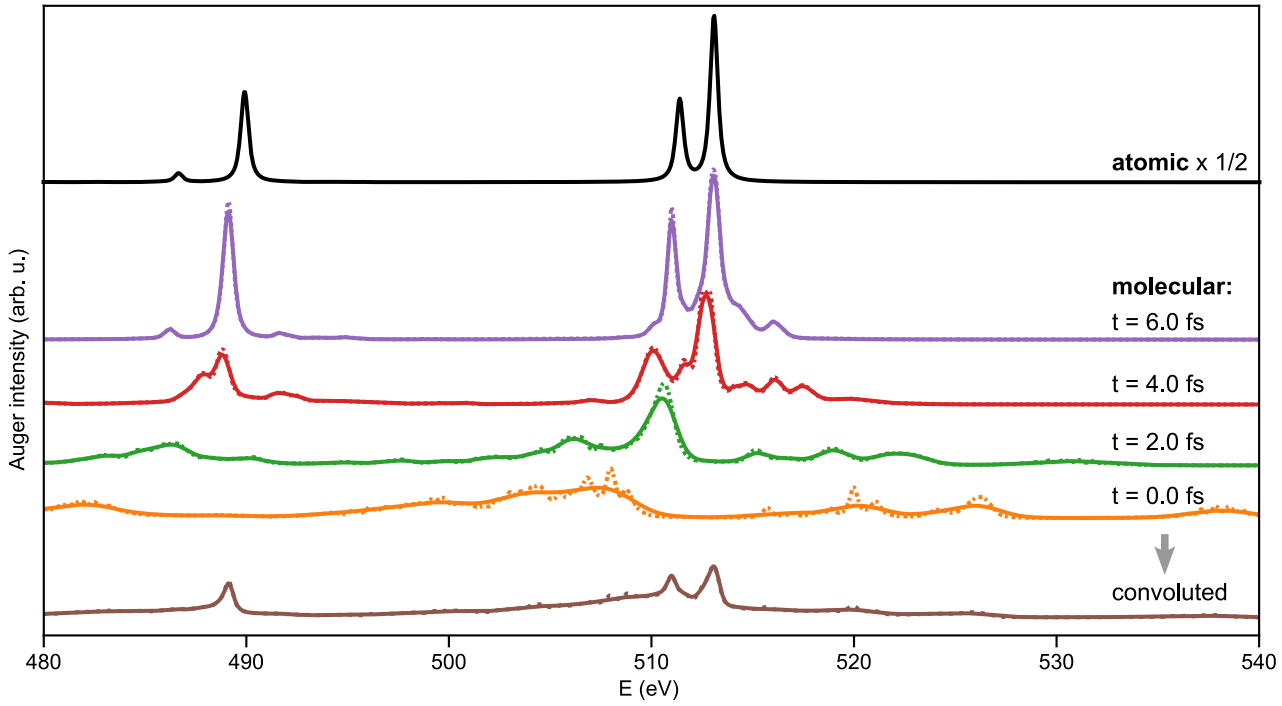


FIG. 4. Emergence of the atomic Auger spectrum from the one-dimensional dynamics model: instantaneous Auger spectra at selected times t according to Eq. (S2) in Supplemental Material [23], the resulting Auger spectrum according to Eq. (S1) in Supplemental Material [23], and the atomic Auger spectrum. The dotted lines show the results obtained without including the additional broadening arising from other vibrational degrees of freedom.

energy curves flatten. One must also consider that an effective broadening arises from the evolving electronic structure during dissociation: the energetic positions of the Auger transitions shift considerably, thereby smearing out the molecular Auger contributions in the final convoluted spectrum. Moreover, the molecular Auger transitions exhibit splitting due to the slightly different electronic character of the oxygen p orbitals, which is reduced as dissociation proceeds. These effects ultimately give rise to much sharper Auger lines for the atomic fragment than for the molecule, rendering the atomic Auger features more prominent in the spectrum. The weak features observed in the experimental spectrum at 515 eV (Fig. 3), together with the broad feature at 505 eV, may therefore be interpreted as remnants of the transient molecular Auger transitions.